


Determining the Thickness of the Dead Layer in Superconducting Film Using a Two-Coil Mutual-Inductance Technique

Ruozhou Zhang^{1,2,†}, Zhanyi Zhao^{1,2,†}, Mingyang Qin^{1,2,*}, Juan Xu¹, Wenxin Cheng^{1,2},
Yangmu Li^{1,2}, Qihong Chen¹, Jie Yuan^{1,3} and Kui Jin^{1,2,3}

¹*Beijing National Laboratory for Condensed Matter Physics, Institute of Physics, Chinese Academy of Sciences, Beijing 100190, China*

²*School of Physical Sciences, University of Chinese Academy of Sciences, Beijing 100049, China*

³*Songshan Lake Materials Laboratory, Dongguan, Guangdong 523808, China*

 (Received 17 March 2022; revised 21 April 2022; accepted 26 April 2022; published 20 May 2022)

A dead layer without superconductivity, i.e., zero resistance and Meissner effect, commonly exists at the interface between substrate and superconducting film. It is demonstrated that the dead layer can significantly degrade the performance of superconducting devices at microwave frequencies. Knowing the thickness of the dead layer, d_{dead} , is necessary when using a two-coil mutual-inductance (TCMI) technique to measure the absolute value of the magnetic penetration depth, λ , in superconducting films. However, there is still no established method to determine d_{dead} in superconducting films. Here, we propose employing the TCMI technique to determine d_{dead} , based on a multilayered model in which the dead layer is sandwiched between superconducting layer and substrate. Using this method, we find that $d_{\text{dead}} = 43 \pm 10$ nm for our superconducting FeSe films, in agreement with the absence of diamagnetism for the 42-nm-thick film. With the d_{dead} determined, we accurately determine the absolute value of λ in superconducting FeSe films.

DOI: [10.1103/PhysRevApplied.17.054034](https://doi.org/10.1103/PhysRevApplied.17.054034)

I. INTRODUCTION

At the film-substrate interface of various functional materials, e.g., ferromagnetic films [1–3], ferroelectric films [4–6], and thermoelectric films [7,8], there commonly exists a dead layer, which exhibits distinct physical properties from the normal layer. Particularly in superconducting films, an interfacial dead layer without zero resistance and Meissner effect usually exists, possibly due to lattice strains, defects, grain boundaries, off stoichiometries, or other growth-related factors [9–13]. It was demonstrated that this dead layer significantly enlarges the effective microwave surface resistance of the systems [10], thus hampering the performance of superconducting devices [14]. Moreover, the thickness of the dead layer is required when measuring the absolute value of the magnetic penetration depth, λ , using techniques such as the two-coil mutual-inductance (TCMI) technique [15,16] and the scanning quantum interference device [17–19].

Until now, there is no established method to determine the thickness of the dead layer in superconducting films, although the scanning transmission electron microscopy [11] and the spatially resolved electron energy-loss

spectroscopy [20,21] can provide useful information by detecting the deviation of crystalline structure, stoichiometry, and valency at the film-substrate interface. Fortunately, the diamagnetic response of superconductors can deliver the information of the superconducting volume fraction [22–24]. Hence, the thickness of the dead layer could be measured in principle through magnetic measurements. Among various magnetic measurement techniques [19,25–28], the TCMI technique has intrigued increasing attention for its simplicity and flexibility [12,15,16,29–36]. What is more, owing to its high sensitivity, the TCMI technique can even be used to detect the diamagnetic screening effect of one single copper-oxygen plane [12] and the monolayer FeSe film [37,38].

In this study, we propose employing the TCMI technique to determine the thickness of the dead layer in superconducting films, based on a multilayered model in which the dead layer is sandwiched between superconducting layer and substrate. A series of superconducting FeSe films are fabricated and characterized to verify the validity of the model.

II. MODEL

In general, a TCMI system consists of a drive coil and a pickup coil, located on opposite sides of the superconducting film, as shown in the inset of Fig. 1(a).

*mingyangqin@iphy.ac.cn

†These authors contributed equally to this work.

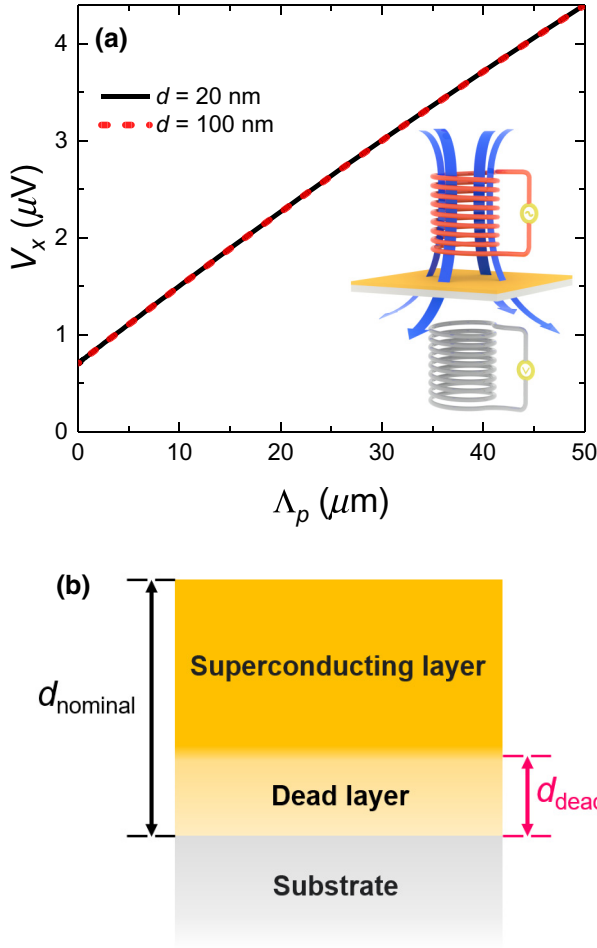


FIG. 1. (a) The induced pickup coil voltage, V_p , as a function of the Pearl penetration depth, Λ_p , calculated for films with $d = 20$ nm (black solid curve) and 100 nm (red dash curve) using the FWC method [32]. The inset shows the schematic illustration of the TCMI device. (b) Schematic of the SDS model.

A magnetic field is produced by the alternating current in the drive coil, which generates an induced pickup coil voltage, $V = V_x + iV_y$, where V_x and V_y represent the in-phase and out-of-phase components, respectively. When the film enters the superconducting state, the magnetic field will be screened [indicated by blue arrows in Fig. 1(a)], reflected as a sudden drop of V_x . As known, the intrinsic length scale of the magnetic screening for a superconducting film is the Pearl penetration depth [18,39],

$$\Lambda_p = \frac{2\lambda^2}{d}, \quad (1)$$

where d is the thickness of the superconducting film. Hence, it is reasonable to conclude that V_x is determined by Λ_p .

To verify this point, the dependence of V_x on Λ_p for 5×5 mm² films with $d = 20$ nm and 100 nm are calculated

using the fast wavelet collocation (FWC) method as follows [32]. According to classical electrodynamics [40], the V_x is determined by the currents, which contain two types for the TCMI system. One is the current in the drive coil, whose contribution to V_x could be calculated based on the coil parameters. In our case, the copper wire diameter is $40 \mu\text{m}$, the inner diameter is 0.5 mm, the outer diameter is 1.3 mm, the length is 1.6 mm, and the separation between two coils is approximately 1 mm. The other is the screening current density in the film, \mathbf{j}_s , which relates to Λ_p through [41,42]

$$\mathbf{j}_s(\mathbf{r}) + \frac{\sinh(\sqrt{2d/\Lambda_p})}{4\pi\sqrt{\Lambda_p d/2}} \int_{\Omega} d^2\mathbf{r}' \frac{\mathbf{j}_s(\mathbf{r}')}{|\mathbf{r} - \mathbf{r}'|} = -\frac{2}{\mu_0\Lambda_p d} \mathbf{A}_d(\mathbf{r}), \quad (2)$$

where Ω is the projection of the film on the x - y plane (film surface), $\mathbf{r} = x\hat{\mathbf{x}} + y\hat{\mathbf{y}}$, μ_0 is the vacuum permeability, and \mathbf{A}_d is the vector potential generated by the drive current. Equation (2) is a two-dimensional Fredholm integral equation, which could be accurately solved by the FWC algorithm [43–45]. More details for this procedure could be found in previous work [32]. The calculation results show that V_x versus Λ_p curves for films with different thickness are indeed identical [see Fig. 1(a)]. Thus, one can extract Λ_p from V_x regardless of the film thickness.

Note that d in Eq. (1) represents the thickness of the superconducting layer, which usually deviates from the nominal film thickness, d_{nominal} , due to the existence of the dead layer. Therefore, we propose a simple multilayered model in which the dead layer with thickness of d_{dead} is sandwiched between superconducting layer and substrate [see Fig. 1(b)], referred to as the superconducting layer-dead layer-substrate (SDS) model below. In this case, Λ_p^{-1} can be expressed as

$$\Lambda_p^{-1} = \frac{1}{2\lambda^2} (d_{\text{nominal}} - d_{\text{dead}}). \quad (3)$$

Equation (3) shows a linear dependence of Λ_p^{-1} on d_{nominal} , of which the slope is $1/2\lambda^2$ and the horizontal intercept is d_{dead} . Hence, one can obtain d_{dead} by fitting the experimental Λ_p^{-1} data for a series of samples with different d_{nominal} . Additionally, λ could be simultaneously determined as

$$\lambda = \sqrt{\frac{d_{\text{nominal}} - d_{\text{dead}}}{2\Lambda_p^{-1}}}. \quad (4)$$

It is worth mentioning that the linear dependence indicated by Eq. (3) holds only for a fixed λ . Considering the scaling law between λ and the superconducting critical temperature, T_c [16,35,46,47], T_c of samples with different d_{nominal} should be the same when applying the SDS model to extract d_{dead} . Besides, Λ_p^{-1} is directly proportional to

the superfluid density, n_s [16], thus d_{dead} extracted using the SDS model represents the thickness of the layer with $n_s \approx 0$.

Experimentally, in order to obtain samples with different d_{nominal} , one can reduce the film thickness using top-down techniques such as the Ar ion milling [10,48,49] or the electrochemically etching technique [50]. However, the etching process may change the T_c of superconducting films [50–53]. In this study, we carry out the bottom-up synthesizing techniques to fabricate films with different d_{nominal} .

III. EXPERIMENTAL METHODS

The superconducting β -FeSe films are grown on (001)-oriented LiF substrate with size of $5 \times 5 \text{ mm}^2$ by the pulsed laser deposition (PLD) technique with a 248-nm

KrF excimer laser [54]. The substrates are covered completely by FeSe films. The FeSe polycrystalline target is synthesized by the solid-state reaction method. The laser repetition rate is 2 Hz, the base vacuum of deposition chamber is 10^{-8} Torr [55], the substrate temperature is kept at 350°C , and the deposition rate is approximately 300 nm h^{-1} . By varying the deposition time, we fabricate a series of films with $d_{\text{nominal}} = 218, 190, 179, 163, 138, 120, 116, 42, \text{ and } 30 \text{ nm}$, respectively (denoted as S1 to S9 below).

X-ray diffraction (XRD) patterns are measured using a SmartLab diffractometer with a Ge (220) crystal monochromator. The nominal film thickness, d_{nominal} , is characterized by a Hitachi SU5000 field-emission scanning electron microscope (SEM). The atomic ratio of Fe to Se is evaluated using the energy dispersive x-ray spectra (EDX) in the same SEM. The resistance is measured

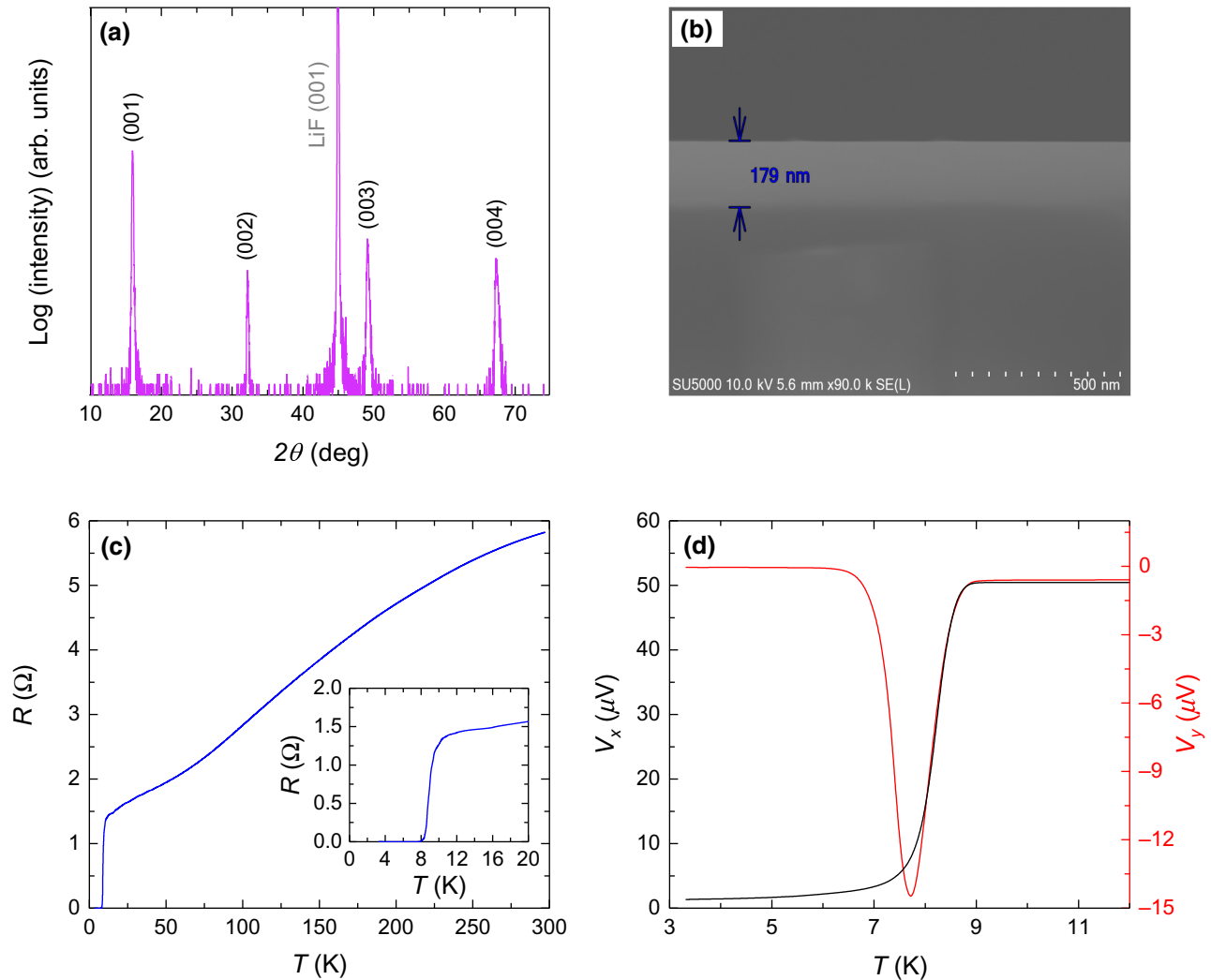


FIG. 2. Crystalline structure, cross-section image, electrical transport property, and diamagnetic response of the typical superconducting FeSe film. (a) Out-of-plane XRD pattern. (b) SEM cross-section image. (c) Temperature-dependent resistance. (d) Temperature dependence of the induced pickup coil voltage. The black and red curves represent the in-phase and out-of-phase components of the pickup coil voltage, respectively.

in a four-terminal configuration. The magnetic measurements are achieved using a homemade TCMI device [22,24,32,56]. A Stanford Research SR830 lock-in amplifier is used to supply an alternating current to the drive coil. The current amplitude is 0.2 mA and the frequency is 50 kHz, producing an approximately 90 μT magnetic field at the film center. The induced pickup coil voltage, $V = V_x + iV_y$, is measured by the same lock-in amplifier with a reference phase of 90° .

Figure 2 summarizes the characterization results of one typical FeSe film with $d_{\text{nominal}} = 179 \pm 10$ nm [see the SEM cross-section image in Fig. 2(b)]. The high-quality (00l)-orientated growth is verified by the XRD θ - 2θ scan, as shown in Fig. 2(a). The temperature-dependent resistance depicted in Fig. 2(c) shows $T_c \sim 8$ K, which is consistent with the onset temperature of the diamagnetic response in V_x [see the black curve in Fig. 2(d)]. The V_y shows a clear dip around T_c , whose full width at half maximum is less than 0.9 K [see the red curve in Fig. 2(d)], indicating good film homogeneity [33].

IV. RESULTS AND DISCUSSION

A. Diamagnetic response of FeSe films with different nominal thickness

In order to verify the validity of the SDS model, we measure the temperature dependence of the induced pickup coil voltage for FeSe films with different d_{nominal} using a homemade TCMI device, as shown in Fig. 3(a). For S1 to S7, the strong diamagnetic response emerges at T_c , indicating large superconducting volume fractions. By contrast, the diamagnetism is extremely weak for S8 ($d_{\text{nominal}} = 42$ nm) and completely vanishes for S9 ($d_{\text{nominal}} = 30$ nm). This indicates low superconducting volume fractions for S8 and S9, suggesting that d_{dead} is about 40 nm for our FeSe films.

Then, the temperature-dependent Λ_p of S1 to S9 is extracted using the FWC method. Considering that Λ_p for S8 and S9 is almost infinite, we show only the data of S1 to S7 in Fig. 3(b).

B. Pearl penetration depth versus nominal thickness

Figure 4(a) presents $\Lambda_p^{-1}(T = 3.6$ K) versus d_{nominal} of FeSe films. For S1 to S7, the data show a clear linearity, which is consistent with the prediction of the SDS model [see Eq. (3)]. Note that, the change of T_c for these films is less than approximately 1 K [see Fig. 3(a)], satisfying the condition for employing the SDS model to determine d_{dead} . We extract d_{dead} through the linear fit, which is 43 ± 10 nm [see the shadow region in Fig. 4(a)], in agreement with the vanished diamagnetism for S8 and S9 [see Fig. 3(a)].

In addition, we use Eq. (4) to calculate the temperature-dependent λ of S7 with $d_{\text{dead}} = 0$ nm (i.e., ignoring the dead layer, black circles) and 43 nm (red circles), respectively. Two curves exhibit non-negligible deviations

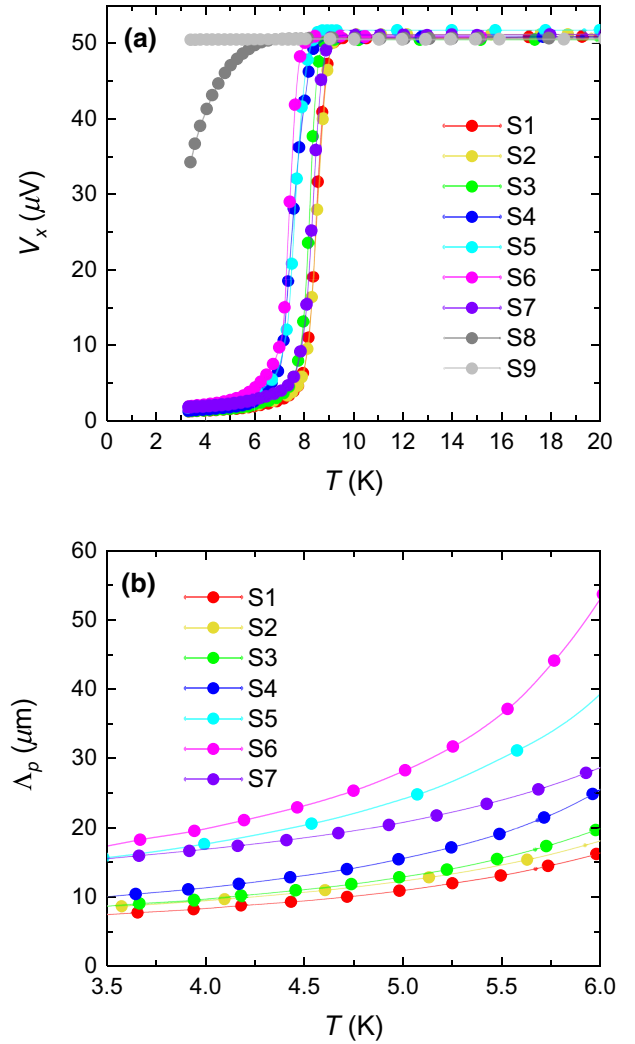


FIG. 3. Temperature dependence of (a) the in-phase component of the pickup coil voltage and (b) the Pearl penetration depth for FeSe films with different d_{nominal} . The films are denoted as S1 to S9, corresponding to $d_{\text{nominal}} = 218, 190, 179, 163, 138, 120, 116, 42,$ and 30 nm, respectively.

below T_c , as shown in Fig. 4(b). Furthermore, we obtain $\lambda(T \rightarrow 0)$ by fitting the low-temperature data using the nodeless gap formula [33,57,58]:

$$\frac{\lambda^{-2}(T)}{\lambda^{-2}(0)} \sim 1 - Ce^{-D/t}, \quad (5)$$

where C is a constant, D is proportional to the minimum gap value, and $t = T/T_c$. As shown in the inset of Fig. 4(b), $\lambda(T \rightarrow 0) = 830$ nm for $d_{\text{dead}} = 0$ nm, and $\lambda(T \rightarrow 0) = 660$ nm for $d_{\text{dead}} = 43$ nm. In other words, ignoring the dead layer may bring an error of approximately 25%.

Actually, the largest error when determining λ using the TCMI technique comes from the dead layer [16,30]. In previous reports, the widely used solution is a growing complex interfacial buffer layer to suppress the dead

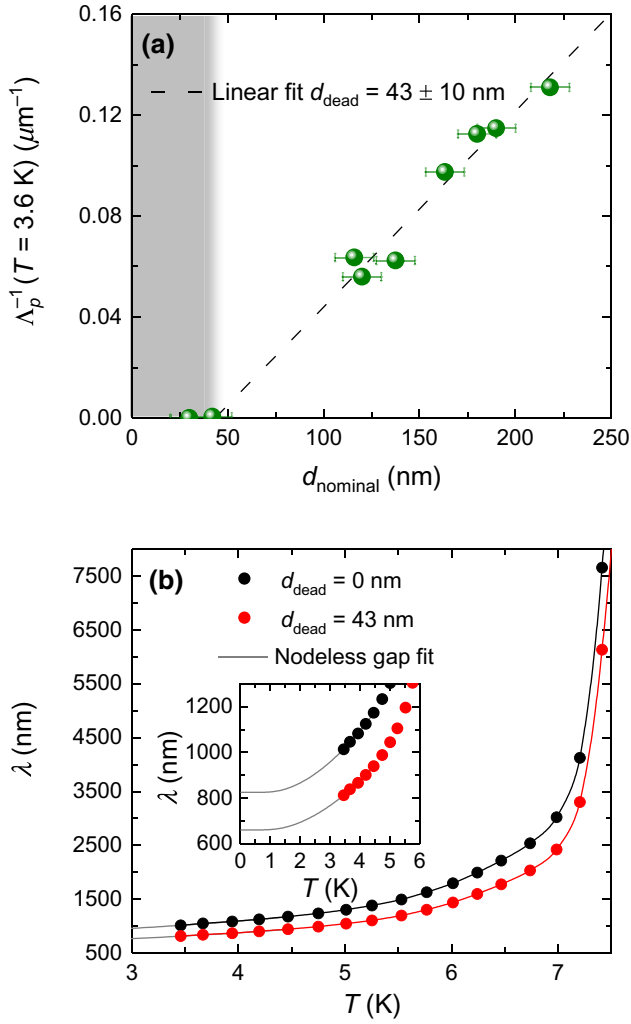


FIG. 4. (a) $\Lambda_p^{-1}(T = 3.6\text{ K})$ versus d_{nominal} of FeSe films. The dashed line is the linear fit to the data of S1 to S7, giving $d_{\text{dead}} = 43 \pm 10\text{ nm}$. The shadow region indicates where the superconductivity vanishes. (b) The temperature-dependent magnetic penetration depth of S7 calculated with $d_{\text{dead}} = 0\text{ nm}$ (black circles) and 43 nm (red circles) using Eq. (4). Gray curves represent nodeless gap fittings using Eq. (5).

layer through advanced synthesis techniques, such as the atomic layer-by-layer molecular beam epitaxy [12,16]. Here, we emphasize that one can easily achieve high-accuracy λ measurements using the SDS model, promising high-efficiency superconductivity research [59–61].

C. Possible origin of the dead layer in FeSe films

Finally, we investigate the possible origin of the dead layer in FeSe films grown on LiF substrates. We present the normalized resistance, $R(T)/R(295\text{ K})$, versus temperature for films with different d_{nominal} in Fig. 5(a). It is shown that the metallicity of films [quantified as $R(295\text{ K})/R(20\text{ K})$] (black triangles) in Fig. 5(b)] decreases rapidly around 40 nm . Meanwhile, the relative atomic ratio

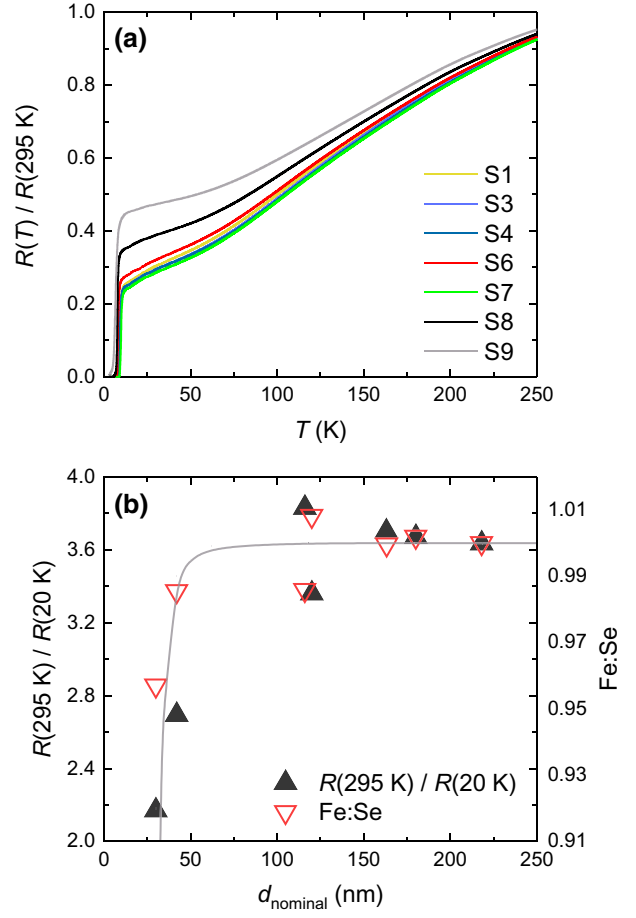


FIG. 5. (a) Temperature-dependent $R(T)/R(295\text{ K})$ of FeSe films with different d_{nominal} . (b) Evolution of $R(295\text{ K})/R(20\text{ K})$ and Fe:Se (relative atomic ratio of Fe to Se with respect to S1) with d_{nominal} . The gray curve is a guide for eye.

of Fe to Se with respect to S1 (denoted as Fe:Se, red triangles) revealed by EDX shows the same tendency with $R(295\text{ K})/R(20\text{ K})$, as depicted in Fig. 5(b). The reduced metallicity combined with the Fe deficiency for small-thickness films is reminiscent of the Fe vacancies induced insulativity in previous reports [24,62]. Moreover, it is demonstrated that the superconductivity of FeSe bulk can be destroyed by minute changes in stoichiometry [13,63]. Therefore, we conclude that the Fe deficiency near the FeSe-LiF interface plays a dominant role in the formation of the dead layer.

V. CONCLUSIONS

In summary, we employ the two-coil mutual-inductance technique to determine the thickness of the dead layer, d_{dead} , in superconducting films, based on the superconducting layer-dead layer-substrate model. In order to check the model, we fabricate and characterize a series of superconducting FeSe films with different nominal thickness. It is found that $d_{\text{dead}} = 43 \pm 10\text{ nm}$ for our FeSe films,

in agreement with the absence of diamagnetism for the 42-nm-thick film. Using this noncontact method, one can easily measure d_{dead} in superconducting films. Moreover, the accurate value of the magnetic penetration depth, λ , can be simultaneously obtained, avoiding an error of approximately 25% from the dead layer. Our study provides an efficient method to measure λ in superconducting films, conducive to exploring the scaling law between λ and T_c in unconventional superconductors [22,64,65].

ACKNOWLEDGMENTS

The authors thank Xiaodong Yu for useful discussions. This work is supported by the National Key Basic Research Program of China (Grants No. 2021YFA0718700, No. 2018YFB0704102, No. 2017YFA0302902, No. 2017YFA0303003, and No. 2016YFA0300301), the National Natural Science Foundation of China (Grants No. 11927808, No. 11834016, No. 118115301, No. 119611410, and No. 11961141008), the Key Research Program of Frontier Sciences, CAS (Grants No. QYZDB-SSW-SLH008 and No. QYZDY-SSW-SLH001), the Strategic Priority Research Program (B) of Chinese Academy of Sciences (Grants No. XDB25000000 and No. XDB33000000), the Beijing Natural Science Foundation (Grant No. Z190008), the Key Area Research and Development Program of Guangdong Province (Grant No. 2020B0101340002), and the CAS Interdisciplinary Innovation Team.

-
- [1] J. Z. Sun, D. W. Abraham, R. A. Rao, and C. B. Eom, Thickness-dependent magnetotransport in ultrathin manganese films, *Appl. Phys. Lett.* **74**, 3017 (1999).
- [2] A. Zakharova, M. Caputo, E. B. Guedes, M. Radovic, F. Nolting, and C. Piamonteze, Interplay between magnetism and interface-induced effects in ultrathin manganites, *Phys. Rev. Mater.* **5**, 124404 (2021).
- [3] W. Luo, S. J. Pennycook, and S. T. Pantelides, Magnetic “Dead” Layer at a Complex Oxide Interface, *Phys. Rev. Lett.* **101**, 247204 (2008).
- [4] L. J. Sinnamon, M. M. Saad, R. M. Bowman, and J. M. Gregg, Exploring grain size as a cause for “dead-layer” effects in thin film capacitors, *Appl. Phys. Lett.* **81**, 703 (2002).
- [5] M. Stengel and N. A. Spaldin, Origin of the dielectric dead layer in nanoscale capacitors, *Nature* **443**, 679 (2006).
- [6] Y. Wang, M. K. Niranjana, K. Janicka, J. P. Velev, M. Y. Zhuravlev, S. S. Jaswal, and E. Y. Tsymlal, Ferroelectric dead layer driven by a polar interface, *Phys. Rev. B* **82**, 094114 (2010).
- [7] Z. Gao, X. Ning, J. Wang, J. Wang, and S. Wang, Ultrahigh power factor and ultralow thermal conductivity at room temperature in PbSe/SnSe superlattice: Role of quantum-well effect, *Small* **18**, 2104916 (2022).
- [8] M. Soroka, K. Knizek, Z. Jirak, P. Levinsky, M. Jarosova, J. Bursik, and J. Hejtmanek, Anomalous Nernst effect in the ceramic and thin film samples of $\text{La}_{0.7}\text{Sr}_{0.3}\text{CoO}_3$ perovskite, *Phys. Rev. Mater.* **5**, 035401 (2021).
- [9] Y. F. Nie, E. Brahim, J. I. Budnick, W. A. Hines, M. Jain, and B. O. Wells, Suppression of superconductivity in FeSe films under tensile strain, *Appl. Phys. Lett.* **94**, 242505 (2009).
- [10] S. Y. Lee, J. H. Lee, J. S. Ryu, J. Lim, S. H. Moon, H. N. Lee, H. G. Kim, and B. Oh, Significant reduction of the microwave surface resistance of MgB_2 films by surface ion milling, *Appl. Phys. Lett.* **79**, 3299 (2001).
- [11] W. Qiu, Z. Ma, D. Patel, L. Sang, C. Cai, M. Shahriar Al Hossain, Z. Cheng, X. Wang, and S. X. Dou, The interface structure of FeSe thin film on CaF_2 substrate and its influence on the superconducting performance, *ACS Appl. Mater. Interfaces* **9**, 37446 (2017).
- [12] G. Logvenov, A. Gozar, and I. Bozovic, High-temperature superconductivity in a single copper-oxygen plane, *Science* **326**, 699 (2009).
- [13] T. M. McQueen, Q. Huang, V. Ksenofontov, C. Felser, Q. Xu, H. Zandbergen, Y. S. Hor, J. Allred, A. J. Williams, D. Qu, J. Checkelsky, N. P. Ong, and R. J. Cava, Extreme sensitivity of superconductivity to stoichiometry in $\text{Fe}_{1+\delta}\text{Se}$, *Phys. Rev. B* **79**, 014522 (2009).
- [14] A. Gurevich, Theory of RF superconductivity for resonant cavities, *Supercond. Sci. Technol.* **30**, 034004 (2017).
- [15] A. T. Fiory, A. F. Hebard, P. M. Mankiewich, and R. E. Howard, Penetration depths of high T_c films measured by two-coil mutual inductances, *Appl. Phys. Lett.* **52**, 2165 (1988).
- [16] I. Bozovic, X. He, J. Wu, and A. T. Bollinger, Dependence of the critical temperature in overdoped copper oxides on superfluid density, *Nature* **536**, 309 (2016).
- [17] J. R. Kirtley, B. Kalisky, J. A. Bert, C. Bell, M. Kim, Y. Hikita, H. Y. Hwang, J. H. Ngai, Y. Segal, F. J. Walker, C. H. Ahn, and K. A. Moler, Scanning SQUID susceptometry of a paramagnetic superconductor, *Phys. Rev. B* **85**, 224518 (2012).
- [18] C. Herrera, J. Franklin, I. Bozovic, X. He, and I. Sochnikov, Scanning SQUID characterization of extremely overdoped $\text{La}_{2-x}\text{Sr}_x\text{CuO}_4$, *Phys. Rev. B* **103**, 024528 (2021).
- [19] J. R. Kirtley, Fundamental studies of superconductors using scanning magnetic imaging, *Rep. Prog. Phys.* **73**, 126501 (2010).
- [20] W. Hu, Z. Feng, B. C. Gong, G. He, D. Li, M. Qin, Y. Shi, Q. Li, Q. Zhang, J. Yuan, B. Zhu, K. Liu, T. Xiang, L. Gu, F. Zhou, X. Dong, Z. Zhao, and K. Jin, Emergent superconductivity in single-crystalline MgTi_2O_4 films via structural engineering, *Phys. Rev. B* **101**, 220510(R) (2020).
- [21] X. Wei, *et al.*, A selective control of volatile and non-volatile superconductivity in an insulating copper oxide via ionic liquid gating, *Sci. Bull.* **65**, 1607 (2020).
- [22] M. Qin, R. Zhang, Z. Lin, Z. Feng, X. Wei, S. Blanco Alvarez, C. Dong, A. V. Silhanek, B. Zhu, J. Yuan, Q. Qin, and K. Jin, In situ magnetic measurements of ionic-liquid-gated superconducting films, *J. Supercond. Novel Magn.* **33**, 159 (2020).
- [23] A. R. Kortan, N. Kopylov, S. Glarum, E. M. Gyorgy, A. P. Ramirez, R. M. Fleming, O. Zhou, F. A. Thiel, P. L. Trevor, and R. C. Haddon, Superconductivity in barium fulleride, *Nature* **360**, 566 (1992).

- [24] M. Qin, X. Jiang, L. Zhang, R. Zhang, F. Chen, J. Xu, Z. Wei, P. Xiong, X. Zhang, L. Xu, J. Yuan, B. Zhu, Q. Chen, B. Leridon, K. Jin, and Z. Zhao, Granular metallicity as a minimal normal state for superconductivity, *Phys. Rev. B* **104**, 174511 (2021).
- [25] M. E. Huber, N. C. Koshnick, H. Bluhm, L. J. Archuleta, T. Azaa, P. G. Bjornsson, B. W. Gardner, S. T. Halloran, E. A. Lucero, and K. A. Moler, Gradiometric micro-SQUID susceptometer for scanning measurements of mesoscopic samples, *Rev. Sci. Instrum.* **79**, 053704 (2001).
- [26] R. Liang, D. A. Bonn, W. N. Hardy, and D. Broun, Lower Critical Field and Superfluid Density of Highly Underdoped Single Crystals $\text{YBa}_2\text{Cu}_3\text{O}_{6+x}$, *Phys. Rev. Lett.* **94**, 117001 (2005).
- [27] C. T. V. Degrieff, Tunnel diode oscillator for 0.001 ppm measurements at low temperatures, *Rev. Sci. Instrum.* **46**, 599 (1975).
- [28] L. Luan, O. M. Auslaender, T. M. Lippman, C. W. Hicks, B. Kalisky, J.-H. Chu, J. G. Analytis, I. R. Fisher, J. R. Kirtley, and K. A. Moler, Local measurement of the penetration depth in the pnictide superconductor $\text{Ba}(\text{Fe}_{0.95}\text{Co}_{0.05})_2\text{As}_2$, *Phys. Rev. B* **81**, 100501(R) (2010).
- [29] A. F. Hebard and A. T. Fiory, Evidence for the Kosterlitz-Thouless Transition in Thin Superconducting Aluminum Films, *Phys. Rev. Lett.* **44**, 291 (1980).
- [30] X. He, A. Gozar, R. Sundling, and I. Bozovic, High-precision measurement of magnetic penetration depth in superconducting films, *Rev. Sci. Instrum.* **87**, 113903 (2016).
- [31] M. C. Duan, Z. L. Liu, J. F. Ge, Z. J. Tang, G. Y. Wang, Z. X. Wang, D. Guan, Y. Y. Li, D. Qian, C. Liu, and J. F. Jia, Development of *in situ* two-coil mutual inductance technique in a multifunctional scanning tunneling microscope, *Rev. Sci. Instrum.* **88**, 073902 (2017).
- [32] R. Zhang, M. Qin, L. Zhang, L. You, C. Dong, P. Sha, Q. Chen, J. Yuan, and K. Jin, Determining the absolute value of magnetic penetration depth in small-sized superconducting films, *Supercond. Sci. Technol.* **34**, 085022 (2021).
- [33] J. A. Skinta, M. S. Kim, T. R. Lemberger, T. Greibe, and M. Naito, Evidence for a Transition in the Pairing Symmetry of the Electron-Doped Cuprates $\text{La}_{2-x}\text{Ce}_x\text{CuO}_{4-y}$ and $\text{Pr}_{2-x}\text{Ce}_x\text{CuO}_{4-y}$, *Phys. Rev. Lett.* **88**, 207005 (2002).
- [34] I. Hetel, T. R. Lemberger, and M. Randeria, Quantum critical behaviour in the superfluid density of strongly underdoped ultrathin copper oxide films, *Nat. Phys.* **3**, 700 (2007).
- [35] G. Yao, M. C. Duan, N. Liu, Y. Wu, D. D. Guan, S. Wang, H. Zheng, Y. Y. Li, C. Liu, and J. F. Jia, Diamagnetic Response of Potassium-Adsorbed Multilayer FeSe film, *Phys. Rev. Lett.* **123**, 257001 (2019).
- [36] D. Li, K. Lee, B. Y. Wang, M. Osada, S. Crossley, H. R. Lee, Y. Cui, Y. Hikita, and H. Y. Hwang, Superconductivity in an infinite-layer nickelate, *Nature* **572**, 624 (2019).
- [37] Z. Zhang, Y.-H. Wang, Q. Song, C. Liu, R. Peng, K. A. Moler, D. Feng, and Y. Wang, Onset of the Meissner effect at 65 K in FeSe thin film grown on Nb-doped SrTiO_3 substrate, *Sci. Bull.* **60**, 1301 (2015).
- [38] Y. T. Cui, R. G. Moore, A. M. Zhang, Y. Tian, J. J. Lee, F. T. Schmitt, W. H. Zhang, W. Li, M. Yi, Z. K. Liu, M. Hashimoto, Y. Zhang, D. H. Lu, T. P. Devereaux, L. L. Wang, X. C. Ma, Q. M. Zhang, Q. K. Xue, D. H. Lee, and Z. X. Shen, Interface Ferroelectric Transition Near the Gap-Opening Temperature in a Single-Unit-Cell FeSe Film Grown on Nb-Doped SrTiO_3 Substrate, *Phys. Rev. Lett.* **114**, 037002 (2015).
- [39] J. Pearl, Current distribution in superconducting films carrying quantized fluxoids, *Appl. Phys. Lett.* **5**, 65 (1964).
- [40] J. D. Jackson, *Classical Electrodynamics* (John Wiley and Sons, New York, 1975).
- [41] S. J. Turneaure, E. R. Ulm, and T. R. Lemberger, Numerical modeling of a two-coil apparatus for measuring the magnetic penetration depth in superconducting films and arrays, *J. Appl. Phys.* **79**, 4221 (1996).
- [42] S. J. Turneaure, A. A. Pesetski, and T. R. Lemberger, Numerical modeling and experimental considerations for a two-coil apparatus to measure the complex conductivity of superconducting films, *J. Appl. Phys.* **83**, 4334 (1998).
- [43] Z. Chen, C. A. Micchelli, and Y. Xu, Fast collocation methods for second kind integral equations, *SIAM J. Numer. Anal.* **40**, 344 (2002).
- [44] Y. Wang and Y. Xu, A fast wavelet collocation method for integral equations on polygons, *J. Integr. Equat. Appl.* **17**, 277 (2005).
- [45] Z. Chen, B. Wu, and Y. Xu, Fast collocation methods for high-dimensional weakly singular integral equations, *J. Integr. Eq. Appl.* **20**, 49 (2008).
- [46] Y. J. Uemura, *et al.*, Universal Correlations between T_c and n_s/m^* (Carrier Density over Effective Mass) in High- T_c Cuprate Superconductors, *Phys. Rev. Lett.* **62**, 2317 (1989).
- [47] C. C. Homes, S. V. Dordevic, M. Strongin, D. A. Bonn, R. Liang, W. N. Hardy, S. Komiyama, Y. Ando, G. Yu, N. Kaneko, X. Zhao, M. Greven, D. N. Basov, and T. Timusk, A universal scaling relation in high-temperature superconductors, *Nature* **430**, 539 (2004).
- [48] G. Friedl, B. Roas, M. Römheld, L. Schultz, and W. Jutzi, Transport properties of epitaxial $\text{YBa}_2\text{Cu}_3\text{O}_x$ films at step edges, *Appl. Phys. Lett.* **59**, 2751 (1991).
- [49] Z. J. Chen, D. M. Feldmann, D. C. Larbalestier, T. G. Holesinger, X. Li, W. Zhang, and M. W. Rupich, Top-down and bottom-up through-thickness current anisotropy in a bilayer $\text{YBa}_2\text{Cu}_3\text{O}_{7-x}$ film, *Appl. Phys. Lett.* **91**, 052508 (2007).
- [50] J. Shioyai, Y. Ito, T. Mitsushashi, T. Nojima, and A. Tsukazaki, Electric-field-induced superconductivity in electrochemically etched ultrathin FeSe films on SrTiO_3 and MgO, *Nat. Phys.* **12**, 42 (2015).
- [51] C. Tarantini, M. Putti, A. Gurevich, Y. Shen, R. K. Singh, J. M. Rowell, N. Newman, D. C. Larbalestier, P. Cheng, Y. Jia, and H. H. Wen, Suppression of the Critical Temperature of Superconducting $\text{NdFeAs}(\text{OF})$ Single Crystals by Kondo-Like Defect Sites Induced by α -Particle Irradiation, *Phys. Rev. Lett.* **104**, 087002 (2010).
- [52] T. Ozaki, L. Wu, C. Zhang, J. Jaroszynski, W. Si, J. Zhou, Y. Zhu, and Q. Li, A route for a strong increase of critical current in nanostrained iron-based superconductors, *Nat. Commun.* **7**, 13036 (2016).
- [53] R. Prozorov, M. Konczykowski, M. A. Tanatar, A. Thaler, S. L. Budko, P. C. Canfield, V. Mishra, and P. J. Hirschfeld, Effect of Electron Irradiation on Superconductivity in Single Crystals of $\text{Ba}(\text{Fe}_{1-x}\text{Ru}_x)_2\text{As}_2$ ($x = 0.24$), *Phys. Rev. X* **4**, 041032 (2014).

- [54] Z. Feng, J. Yuan, G. He, W. Hu, Z. Lin, D. Li, X. Jiang, Y. Huang, S. Ni, J. Li, B. Zhu, X. Dong, F. Zhou, H. Wang, Z. Zhao, and K. Jin, Tunable critical temperature for superconductivity in FeSe thin films by pulsed laser deposition, *Sci. Rep.* **8**, 4039 (2018).
- [55] G. He, Z. Wei, Z. Feng, X. Yu, B. Zhu, L. Liu, K. Jin, J. Yuan, and Q. Huan, Combinatorial laser molecular beam epitaxy system integrated with specialized low-temperature scanning tunneling microscopy, *Rev. Sci. Instrum.* **91**, 013904 (2020).
- [56] R. Zhang, M. Qin, L. Zhang, L. You, C. Dong, P. Sha, J. Yuan, and K. Jin, Measurement of magnetic penetration depth in superconducting films by two-coil mutual inductance technique, *Acta Phys. Sin.* **69**, 047401 (2020).
- [57] M. Abdel-Hafez, J. Ge, A. N. Vasiliev, D. A. Chareev, J. Van de Vondel, V. V. Moshchalkov, and A. V. Silhanek, Temperature dependence of lower critical field $H_{c1}(T)$ shows nodeless superconductivity in FeSe, *Phys. Rev. B* **88**, 174512 (2013).
- [58] R. Khasanov, M. Bendele, A. Amato, K. Conder, H. Keller, H. H. Klauss, H. Luetkens, and E. Pomjakushina, Evolution of Two-Gap Behavior of the Superconductor FeSe_{1-x} , *Phys. Rev. Lett.* **104**, 087004 (2010).
- [59] J. Yuan, *et al.*, Scaling of the strange-metal scattering in unconventional superconductors, *Nature* **602**, 431 (2022).
- [60] J. Yuan, V. Stanev, C. Gao, I. Takeuchi, and K. Jin, Recent advances in high-throughput superconductivity research, *Supercond. Sci. Technol.* **32**, 123001 (2019).
- [61] M. Qin, Z. Lin, Z. Wei, B. Zhu, J. Yuan, I. Takeuchi, and K. Jin, High-throughput research on superconductivity, *Chin. Phys. B* **27**, 127402 (2018).
- [62] T. K. Chen, C. C. Chang, H. H. Chang, A. H. Fang, C. H. Wang, W. H. Chao, C. M. Tseng, Y. C. Lee, Y. R. Wu, M. H. Wen, H. Y. Tang, F. R. Chen, M. J. Wang, M. K. Wu, and D. Van Dyck, Fe-vacancy order and superconductivity in tetragonal $\beta\text{-Fe}_{1-x}\text{Se}$, *Proc. Natl. Acad. Sci. USA* **111**, 63 (2014).
- [63] K. Hanzawa, Y. Yamaguchi, Y. Obata, S. Matsuishi, H. Hiramatsu, T. Kamiya, and H. Hosono, Insulator-like behavior coexisting with metallic electronic structure in strained FeSe thin films grown by molecular beam epitaxy, *Phys. Rev. B* **99**, 035148 (2019).
- [64] J. Kinney, J. Garcia-Barriocanal, and A. M. Goldman, Homes scaling in ionic liquid gated $\text{La}_2\text{CuO}_{4+x}$ thin films, *Phys. Rev. B* **92**, 100505(R) (2015).
- [65] A. Rufenacht, J. P. Locquet, J. Fompeyrine, D. Caimi, and P. Martinoli, Electrostatic Modulation of the Superfluid Density in an Ultrathin $\text{La}_{2-x}\text{Sr}_x\text{CuO}_4$ Film, *Phys. Rev. Lett.* **96**, 227002 (2006).